JGR Atmospheres

RESEARCH ARTICLE
10.1029/2024JD041030

Observed Links Between Atmospheric Cloud Radiative Effects and Mesoscale Organization of Deep Convection

Ni Dai[1], Hui Su[2], J. David Neelin[3], Brian J. Soden[4], and Yi-Hung Kuo[3,5]

[1]Joint Institute for Regional Earth System Science & Engineering, University of California, Los Angeles, CA, USA, [2]Department of Civil and Environmental Engineering, Hong Kong University of Science and Technology, Clear Water Bay, Hong Kong, [3]Department of Atmospheric and Oceanic Sciences, University of California, Los Angeles, CA, USA, [4]Rosenstiel School of Marine and Atmospheric Science, University of Miami, Miami, FL, USA, [5]Cooperative Institute for Modeling the Earth System, Princeton University, Princeton, NJ, USA

Abstract Recent research suggests atmospheric cloud radiative effect (ACRE) acts as an important feedback mechanism for enhancing the development of convective self-aggregation in idealized numerical simulations. Here, we seek observational relationships between longwave (LW) ACRE and the spatial organization of mesoscale convective systems (MCSs) in the tropics. Three convective organization metrics that are positively correlated with the area of MCS, that is, convective organization potential, the area fraction of precipitating MCS, and the precipitation fraction of MCS, are used to indicate the degree of convective organization. Our results show that the contrast in the LW ACRE inside and outside an MCS is consistent across different MCS precipitation intensities throughout the life cycle of an MCS, typically 90–100 W/m^2, and provides important positive feedback to the circulation of the given MCS. However, the LW ACRE inside and outside an MCS as well as their difference are not strongly related to the degree of organization, suggesting that the LW cloud radiative feedback may be supportive of MCS formation and maintenance without necessarily being a dominant factor for spatial organization of MCSs. The domain average vertical velocity does tend to be related to the measures of convective organization, suggesting that factors that favor large-scale low-level convergence may exert a leading effect in creating an environment favorable for mesoscale organization of deep convection.

Plain Language Summary The difference between radiative cooling in the dry regions and radiative heating in the moist clusters encourages self-generated radiative circulations in numerical models, which drives scattered moist clusters into organized moist patches. We examine the observed relationship between the spatial organization of mesoscale convective systems (MCSs) and cloud-related radiative heating/cooling. The difference between cloud-related heating inside and outside MCSs is found to be important for the development of individual MCSs, but it still cannot explain the organizational behavior of MCSs in the real world. The organization of MCSs seems to be strongly tied to the external factors in their large-scale environment, such as large-scale low-level convergence.

Key Points:

- Longwave cloud radiative heating observations are consistent with a positive feedback supporting individual mesoscale convective systems (MCSs)
- Observed cloud-related radiative heating does not exert a strong influence on the spatial organization of MCSs
- Observed mesoscale convective organization is closely related to large-scale low-level convergence

Supporting Information:

Supporting Information may be found in the online version of this article.

Correspondence to:

H. Su,
cehsu@ust.hk

Citation:

Dai, N., Su, H., Neelin, J. D., Soden, B. J., & Kuo, Y.-H. (2025). Observed links between atmospheric cloud radiative effects and mesoscale organization of deep convection. *Journal of Geophysical Research: Atmospheres*, *130*, e2024JD041030. https://doi.org/10.1029/2024JD041030

Received 20 FEB 2024
Accepted 13 APR 2025

1. Introduction

Mesoscale convective systems (MCS) are complexes of organized deep convective cloud clusters (e.g., Houze, 1989; Schumacher & Rasmussen, 2020; Trapp, 2013). These systems usually stretch across horizontal scales ranging from hundreds to several thousand kilometers and form extensive, continuous areas of precipitation, which can persist for longer than 6 hours. They contribute a significant portion of the total rainfall in the tropical and midlatitude regions, especially during the warm seasons (Angulo-Umana & Kim, 2023; Feng et al., 2019; Houze, 1989). Convection associated with the MCSs interacts with large-scale circulation through modulating and redistributing the low-level moist entropy or moist static energy (MSE) contributed to the atmosphere via diabatic processes, including radiation and surface fluxes (e.g., Emanuel et al., 1994; Tomassini, 2020). The expansive area of anvil clouds associated with MCSs can also strongly impact the Earth's radiation balance. Therefore, changes in MCS patterns have broader implications for climate variability and change.

In idealized numerical simulations of radiative-convective equilibrium (RCE), isolated convective updrafts tend to self-aggregate into spatially organized clusters despite homogeneous boundary conditions and forcing (e.g., Bretherton et al., 2005; Held et al., 1993; Su et al., 2000). This self-aggregation behavior is relevant to observed phenomena such as MCSs, tropical cyclones, and the Madden-Julian Oscillation (Holloway et al., 2017). The

spatial organization of convection at the mesoscale and synoptic scales has been observed to anti-correlate strongly with mid-to-upper tropospheric relative humidity and cloudiness (Bony et al., 2020; Holloway et al., 2017; Tobin et al., 2012, 2013) and thus can modulate the tropical top-of-atmosphere (TOA) radiation budget through variations in relative humidity and cloudiness (Bony et al., 2020). Observed links between the mesoscale convective organization and changes in tropical precipitation are also strong. The changes in the mean tropical precipitation pattern are highly dependent on the frequency of mesoscale-organized deep convection (Tan et al., 2015). Increases in both the intensity and frequency of heavy precipitation events tend to coincide with a higher degree of mesoscale organized clusters in the tropics (Angulo-Umana & Kim, 2023; Dai & Soden, 2020; Semie & Bony, 2020).

Despite the tendency of intensified heavy rainfall, the overall convective organization scenes found in models and observations are associated with a net loss of LW radiation to the space and a drier mean state (e.g., Bony et al., 2020; Bretherton et al., 2005; Hollway et al., 2017; Tobin et al., 2012; Wing et al., 2017). A plethora of previous studies have investigated the mechanisms behind the development of convective self-aggregation in numerical simulations of RCE (for recent reviews, see, e.g., Muller et al., 2022; Wing et al., 2017). A key process involves the longwave (LW) radiative feedback loop: the contrast between the strong LW radiative cooling in the dry regions and the weakened radiative cooling in the moist regions can drive a low-level vertical circulation, leading to a net import of MSE from dry to moist regions that can further expand the dry regions and enhance the self-aggregation (Bretherton et al., 2005; Muller & Bony, 2015; Muller & Held, 2012). Mechanism-denial experiments have also confirmed that removing the horizontal radiation-cloud-water vapor feedback (i.e., applying a horizontally homogeneous radiation profile to all the atmospheric columns or the boundary layer) inhibits convective self-aggregation in cloud-resolving models (Bretherton et al., 2005; Muller et al., 2022; Yang, 2018a; Yao & Yang, 2023) as well as in general circulation models (GCM; e.g., Arnold & Putman, 2018). Yang (2018a), Muller et al. (2022) emphasized the importance of radiative feedback in the boundary layer for the development of self-aggregation. Yao and Yang (2023) further conducted a vertically resolved MSE analysis, revealing that the radiative cooling in the lower troposphere is the primary contributor to the MSE variance that drives self-aggregation, especially in colder climates (280–290 K). In a GCM, the frequency of a higher degree of large-scale aggregation decreased after suppressing the radiative interactions by prescribing the same atmospheric radiative cooling profile at each time step (Zhang et al., 2021).

LW cloud radiative effect (CRE; Cess et al., 1990), the difference between total-sky LW radiative flux and clear-sky LW flux, is the largest contributor to the changes in radiative fluxes at the TOA and surface in the tropics (e.g., Dai et al., 2021). Mass-weighted vertically integrated atmospheric CRE (ACRE; the difference between CRE at the TOA and surface) is the cloud-related radiative heating and has been observed to balance more than half of the total atmospheric heat transport in the tropical warm pool (10°S–10°N, 150°E–180), to be linked with column relative humidity and tropical precipitation patterns, and to intensify the development of tropical cyclones (Harrop & Hartmann, 2016; Needham & Randall, 2021; Ruppert et al., 2020; Wu et al., 2021). Voigt et al. (2021) reviewed the role played by the ACRE on the tropical circulations based on Phase 6 of the Coupled Model Intercomparison Project (CMIP6; Webb et al., 2017) Clouds On-Off Klimate Model Intercomparison Experiment (COOKIE; Stevens et al., 2012). The cloud-radiative heating/cooling can be switched on and off in these aquaplanet (no land with zonally uniform sea surface temperature imposed) experiments. The ACRE is found to strengthen the Hadley circulation, narrow the Inter-Tropical Convergence Zone (ITCZ) while broadening the tropical descent, and enhance the heavy tropical precipitation (Albern et al., 2018; Benedict et al., 2020; Harrop & Hartmann, 2016; Popp & Silvers, 2017). On smaller scales, previous modeling studies have suggested that the ACRE plays a vital role in the initial formation of tropical convective systems and in maintaining the state of convective self-aggregation (e.g., Bretherton et al., 2005; Miller & Frank, 1993; Muller & Bony, 2015; Muller & Held, 2012; Wing & Emanuel, 2014; Wing et al., 2017; Xu & Randall, 1995).

These pieces of evidence lead to a question that we examine observationally in this study: Could the observed spatial organization of MCSs be enhanced by the LW ACRE? Based on the studies above, the contrast between the cloud-related radiative heating in the MCS regions and radiative cooling in the dry regions may induce and strengthen the thermally direct secondary circulations and transport MSE into the cloudy areas. The interaction between clouds and radiation creates positive feedback, further leading to the development of the spatial organization of MCSs. Note that most of the previous numerical simulations are under non-rotating RCE, characterized by the lack of superimposed large-scale circulations (Emanuel, 2007). Could the LW ACRE have a strong

influence on the observed mesoscale convective organization, with large-scale circulations of longer time scales existing?

Here, we investigate the relationship between the spatial organization of MCSs and the associated LW ACRE as well as the secondary thermally direct circulation. Section 2 describes the satellite/reanalysis data used and the methodology. Section 3 introduces six different convective organization metrics and discusses their applications. The relationships between convective organization, LW ACRE, and vertical velocity for MCS and non-MCS regions are presented in Section 4. Section 5 analyzes the LW ACRE and vertical velocity associated with individual MCSs for strongly and weakly organized cases. The relationships between the convective organization and contrasting LW ACRE between MCS and non-MCS regions are also shown in this section. Section 6 exhibits the temporal evolution of the relationships described in Section 4 and the influence of large-scale convergence on the spatial organization of MCSs. Section 7 summarizes this study.

2. Data and Methodology

2.1. Observations

2.1.1. Hourly SYN1deg LW Radiative Fluxes From CERES

The National Aeronautics and Space Administration (NASA)'s Clouds and the Earth's Radiant Energy System (CERES) Synoptic 1° (SYN1deg-1Hour Edition4.1; Doelling et al., 2016; Wielicki et al., 1996) hourly observed radiative fluxes are used to calculate the observed ACRE. The CERES radiances were observed from Terra, Aqua, and Suomi-National Polar-Orbiting Partnership satellites and were converted into fluxes by incorporating cloud and aerosol properties from the CERES project's Moderate Resolution Imaging Spectroradiometer (MODIS) imager (Doelling et al., 2016; Minnis et al., 2011, 2021 calibrated hourly geostationary satellite (GEO)) imager radiance with the CERES MODIS pixel radiance to estimate the 1°-gridded global TOA, surface, and in-atmosphere LW fluxes via several approaches. The 1-hourly SYN1deg fluxes were then produced through temporal interpolation as well as a series of normalizations. This data set is archived from March 2000 to the present at https://ceres.larc.nasa.gov/.

Only the LW fluxes are considered in this study. The LW CREs at the TOA and surface were calculated as the difference between the total-sky LW flux and clear-sky LW flux at each level. The LW ACRE was calculated as the difference between the LW CRE at the TOA and surface.

2.1.2. IMERG Precipitation

The Global Precipitation Measurement (GPM; Skofronick-Jackson et al., 2017) mission, a collaborative satellite mission initiated by NASA and Japan Aerospace Exploration Agency (JAXA) in February 2014, serves as the successor to the Tropical Rainfall Measuring Mission (TRMM; Simpson et al., 1996). Integrated Multi-satellite Retrievals for the Global Precipitation Measurement (IMERG; Huffman et al., 2014) represent NASA's advanced precipitation algorithm. This algorithm is applied to TRMM and GPM data to compile a satellite precipitation data set from 2000 to the present, featuring a high spatial ($0.1° \times 0.1°$) and temporal (30 min) resolution. The IMERG precipitation data were coarsened to a spatial resolution of $0.25° \times 0.25°$ in this study. The IMERG data set has limited values in the polar regions. More details can be found at https://gpm.nasa.gov/data/imerg.

2.1.3. GPM_MERGIR Brightness Temperature

The NCEP/CPC L3 Half Hourly 4 km Global (60°S–60°N) Merged IR V1 (GPM_MERGIR; Janowiak et al., 2017) brightness temperature (T_b, unit of K) is merged and inter-calibrated from the European, Japanese, and U.S. geostationary satellites every 30 min. This process involves remapping the original satellite infrared data at a pixel resolution of approximately 4 km to a latitude-longitude grid and then applying a zenith angle correction algorithm developed by Joyce et al. (2001). Continuous GPM_MERGIR records began in February 2000. The data can be obtained at https://disc.gsfc.nasa.gov/datasets/GPM_MERGIR_1/summary.

2.2. ERA5 Reanalysis

The ERA5 reanalysis (Hersbach et al., 2020) was released in 2017 by the European Centre for Medium-Range Weather Forecasts (ECMWF) to succeed the ERA-Interim reanalysis (Dee et al., 2011). It is a global

atmospheric reanalysis data set at a high spatio-temporal resolution with long temporal coverage. More than 200 parameters can be obtained hourly at a horizontal resolution of 0.25° × 0.25° on 37 pressure levels, spanning from January 1950 to the present. The ERA5 hourly output is produced in an operational Integrated Forecast System (IFS CY41r2) with improved radiation and convection parameterization schemes, through a 12-hourly 4-dimensional variational assimilation (4D-Var) that integrates model forecast fields with an extensive array of historical satellite and in situ observations. A variational bias correction scheme is applied to adjust for biases in satellite, in situ, and aircraft-measured parameters (e.g., radiance, total column ozone, air temperature, and surface pressure). In this study, hourly vertical pressure velocity (unit of Pa/s) and column water vapor (unit of mm) are from ERA5.

2.3. Definition of MCSs and Its Relationship to ACRE Data

Our MCS detection method is the same as in Schiro et al. (2020). Following Machado and Rossow (1993), the GPM_MERGIR T_b pixels with a brightness temperature lower than 250 K were segregated into clusters in the tropics (24.5°S to 24.5°N) for each hourly snapshot. All clusters do not share any common pixels (Machado & Rossow, 1993; Wielicki & Welch, 1986). To be considered as an MCS, a cluster must cover an area greater than 2,000 km^2 and have one or more T_b pixel values lower than 225 K. We did not differentiate between oceanic and continental MCSs in this study. Similar to Bony et al. (2020), we only considered the hourly snapshots of MCSs with less than 1% of the tropical T_b pixels that are undefined during 01/2001–12/2017 or the total number of MCSs is within two standard deviations of the averaged mean during the period.

MCS pixels were then set as 1, non-MCS pixels as 0, and missing values as NaN to create the MCS masks at the original GPM_MERGIR T_b resolution of ∼4 km. Using the nearest neighbor interpolation, we coarsened the MCS masks to a spatial resolution of 0.25° × 0.25° to match the one of ERA5 reanalysis and coarsened IMERG precipitation. The nearest neighbor interpolation method ensured that the coarsened MCS masks retained all MCS information from the original ∼4 km resolution.

Although the CERES footprint is 25 km in diameter near nadir, CERES fluxes were averaged to 1° × 1° using techniques in Hazra et al. (1993) to alleviate the problem of more footprints overlapping on the boundary of a region than inside of a region. However, such a 1° × 1° resolution of CERES fluxes can be too coarse to study how the ACRE is related to the smallest of the traditionally defined MCSs, being nearly five times larger than the minimum area in the definition above. To address this concern, we excluded the MCS clusters with less than 16 pixels (1° × 1°) in the 0.25° × 0.25° MCS masks when computing the ACRE-related results. These MCS masks were coarsened to 1° × 1° to align with the CERES fluxes.

2.4. Three Diagnostics Based on Domain Selection

We designed three diagnostics in terms of domain selection to study the spatial organization of MCSs (by the organization metrics discussed in Section 3) over a certain domain. The first diagnostic is based on domains of different sizes (i.e., 10° × 10°, 20° × 20°, etc.) that move every 5° longitude and 5° latitude. The second and third use domains centered on the centroid of each MCS and centered on the centroid of the precipitating part of non-MCSs (outside MCS). For each of these three types of domains within the tropics (24.5°S to 24.5°N) at every hour from 01/2001 to 12/2017, we collect the averages of LW ACRE and vertical velocity for the MCS and non-MCS regions as well as the domain-wise degree of convective organization and mean precipitation rate.

3. Convective Organization Metrics

To measure the degree of convective organization for MCSs, we adopt several commonly used metrics and introduce two new ones that highlight the precipitation features of MCSs. As different indices describe different aspects of convective organization, we select the ones that bear a positive relation to the area of MCSs for later parts of this study. This section describes these indices and their characteristics in relation to the size of MCSs.

The Convective Organization Index (Iorg) is one of the most widely used statistical metrics to measure whether the convective systems over a certain size of the domain are aggregated or disaggregated (Bony et al., 2020; Tompkins & Semie, 2017). Here, we followed the method described in Bony et al. (2020) and computed the Iorg with our hourly 0.25° × 0.25° MCS mask. The distances among the MCSs are sorted and evaluated against a

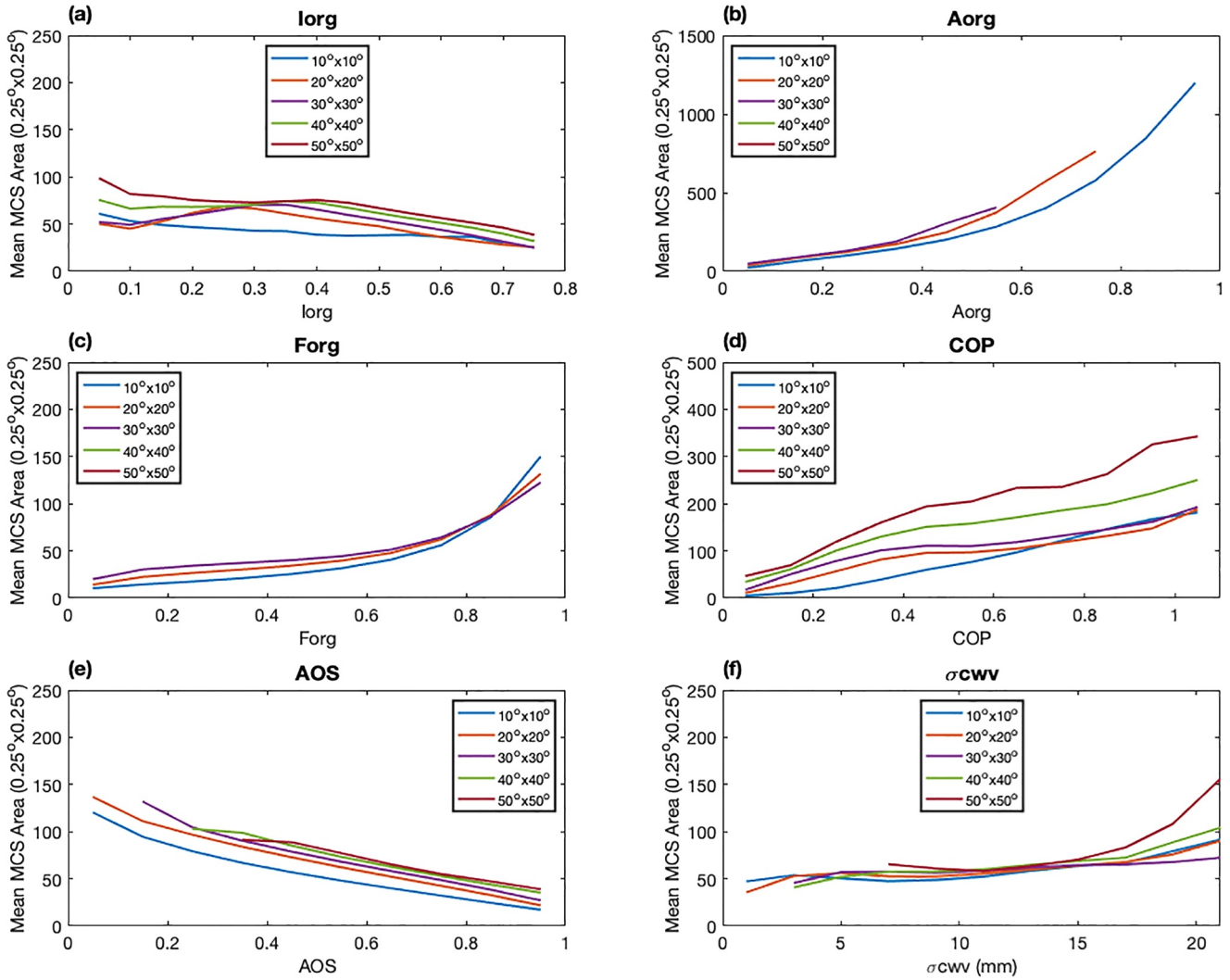

Figure 1. Relationship between each of the six convective aggregation metrics and the averaged area of MCSs (measured in the number of 0.25° × 0.25° pixels) over five sizes of the domain. The six convective aggregation metrics are (a) Iorg (Convective Aggregation Index), (b) Aorg (the fraction of precipitating area of MCS), (c) Forg (the precipitation fraction of MCS), (d) COP (Convective Organization Potential), (e) AOS (area fraction of subsidence), and (f) σCWV (spatial variance of column water vapor). The five domain sizes are 10° × 10° (blue), 20° × 20° (orange), 30° × 30° (purple), 40° × 40° (green), and 50° × 50° (red). The domains are taken each 5° longitude and 5° latitude. All MCSs regardless of size were considered when computing Iorg, Aorg, Forg, and COP.

random Poisson distribution with the total number of the MCSs within a domain. The value of Iorg is very simple to interpret: Iorg larger (smaller) than 0.5 is considered to be clustered (dispersed).

We note that Iorg only considers the distances among the MCSs but not their horizontal areas. As Figure 1a shows, the mean area of MCSs over a domain tends to decrease as Iorg increases when the MCSs are supposed to be clustered (indicated by Iorg being greater than 0.5). This is counterintuitive, as more organized systems can be larger. Previous observations suggest that convective systems can interact with each other and grow in size. Zhu et al. (1992) analyzed the Landsat, Advanced Very High-Resolution Radiometer (AVHRR), and Skylab data and discovered that large cumulus clouds can encourage the development of other large ones nearby. It is also known that, through cold pool interactions, cloud size, and proximity can increase the potential for convective organization (e.g., Feng et al., 2015).

Convective organization potential (COP), introduced by White et al. (2018), focuses on the interaction potential among the convective systems. This potential is calculated by considering the total number of convective systems over a certain domain, the distance among them, and the area of the systems. Following White et al. (2018), we applied this COP metric to our MCS mask. Higher (Lower) COP suggests that the MCSs are respectively larger

(or smaller) and situated closer to (or farther from) one another, and therefore, are more likely to interact with each other horizontally over a domain. Although the majority of the COP values are under 1 when studying the observed convective systems, the values can reach several hundred in some cases.

Besides these statistical convective organization metrics, the spatial organization of convection can also be characterized using fractions of subsidence or precipitation. For example, convective organization can be manifested in changes in the area fraction of subsidence (AOS) measured by the ERA5 vertical velocity at 500 hPa. Over a domain that is large enough to track the complete vertical circulations associated with all the convective systems existing, the stronger the organization of deep convection, the larger the area fraction of subsidence.

The spatial variance of vertically integrated moist static energy (MSE) has also been widely used to quantify the degree of convective self-aggregation (e.g., Wing & Emanuel, 2014). Similarly, the spatial variance of column water vapor (CWV) from ERA5 can also characterize the behavior of aggregation as the spatial variations of MSE in the tropics are mostly contributed by variations of CWV due to a weak temperature gradient (Dai & Soden, 2020).

Since we are interested in whether the LW ACRE plays a role in the development of individual MCSs and the spatial organization among them, we construct two other convective organization metrics that are further indicative of the intensity of interactive MCSs over a domain: the precipitation fraction of MCS (Forg) and the fraction of precipitating area of MCS (Aorg). Forg is defined as the ratio of the sum of the precipitation rate of MCSs to the total precipitation rate over the same domain. The hourly precipitation rate (mm/hr) is from IMERG and has been coarsened to the same horizontal resolution as in ERA5. Aorg is simply defined as the ratio of the number of the precipitating grid points of MCSs to the total number of grid points of a domain. Both Forg and Aorg increase with the intensity of MCS-averaged precipitation over the same domain, as well as with the domain-mean precipitation (e.g., Figure S1 in Supporting Information S1).

Figure 1 shows how the averaged MCS area varies with these six convective organization metrics over domains of different sizes ranging from 10° × 10°–50° × 50°. Both Aorg (Figure 1b) and Forg (Figure 1c) increase exponentially with the mean area of MCSs over the domain, indicating a fast expansion of the MCS horizontal size as the fraction of the raining area or rain amount from MCSs increases. Among the other four convective organization metrics, COP (Figure 1d) is the only one that exhibits a positive relationship with the averaged area of MCSs. The domain-averaged area of MCSs almost linearly increases with the interaction potential among the MCSs: the closer the MCSs are, the larger and more developed MCSs will be.

For the other three metrics, Iorg (Figure 1a) does not increase with the domain-averaged area of MCSs and even decreases with it when MCSs over the domain are more organized (i.e., Iorg >0.5). AOS (Figure 1e) exhibits an almost linearly negative relationship with the averaged MCS area. This might be caused by the limited size of the domains relative to the size of MCSs in the tropics: as the horizontal radius of the majority of the MCSs ranges from 100 to 5,000 km, our analysis domains of 10° × 10°–50° × 50° do not encompass the full subsidence areas surrounding the MCSs. Furthermore, the domain-averaged area of MCSs around 1.77° × 1.77° (50 0.25° × 0.25° grid boxes) does not increase with σ CWV (Figure 1f) until σ CWV is larger than about 17 mm, suggesting that σ CWV is only a good indicator of the organization of MCSs when the averaged MCSs over the domain are sufficiently large. Therefore, we only use COP, Forg (the fraction of MCS precipitation), and Aorg (the precipitating area fraction of MCS) in this study.

As previously mentioned, Frog and Aorg are strongly associated with domain-mean precipitation, unlike the convective aggregation indices commonly used in RCE studies (e.g., Wing et al., 2020). The relationship between COP and MCS-averaged or domain-mean precipitation (Figure S2 in Supporting Information S1) shows diminishing increases across the COP bins from 0%–10% to 90%–100% (except for the 90%–100% bar for domain-mean precipitation), in contrast to the more linear relationship observed for Forg and Aorg (e.g., Figure S1 in Supporting Information S1). This result aligns with the findings of White et al. (2018). Previous studies (Chou et al., 2012; Emori & Brown, 2005; O'Gorman & Schneider, 2009) have shown that larger precipitation intensity is associated with stronger upward motion, as inferred from the moisture budget. In our study, the domain-mean precipitation is proportional to the vertical ascent—measured by vertical velocity at 500 hPa (ω_{500})—in both the MCS and non-MCS regions in the same domain (Figure S3 in Supporting Information S1). In the next section, we will explore how the three organization indices (Forg, Aorg, and COP) relate to the vertical circulation between the MCS and non-MCS regions.

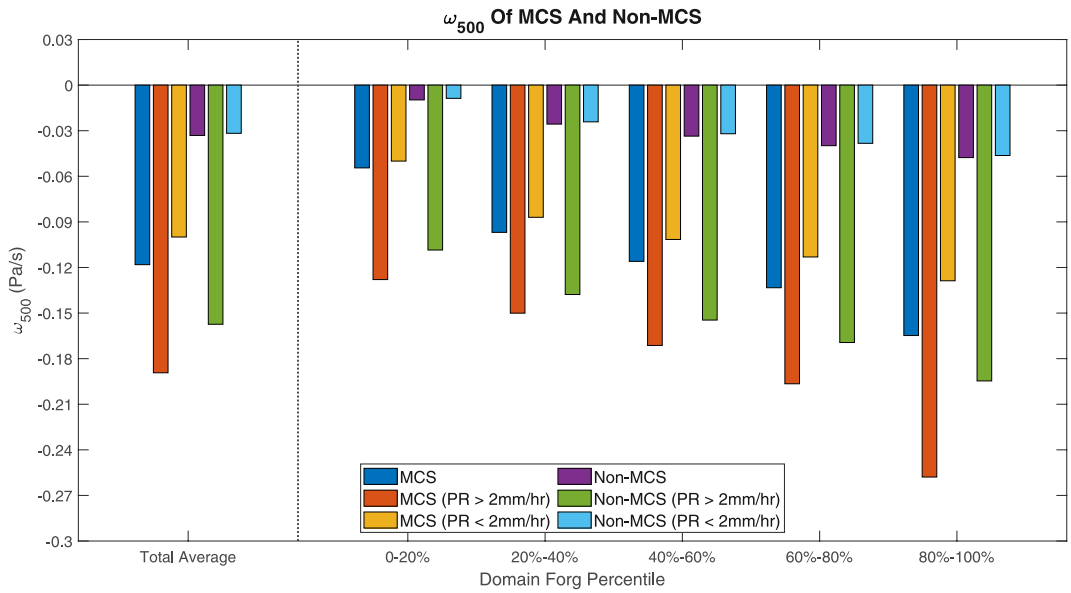

Figure 2. Averaged vertical pressure velocity at 500 hPa (ω_{500} Pa/s) as a function of the percentiles of Forg over 10° × 10° domains, divided into contributions as follows: MCS (blue), MCS with precipitation rate larger than 2 mm/hr (red), MCS with precipitation rate smaller than 2 mm/hr (yellow), non-MCS (purple), non-MCS with precipitation rate larger than 2 mm/hr (green), and non-MCS with precipitation smaller than 2 mm/hr (cyan). Each domain is centered on a centroid of an MCS larger than 16 0.25° (around 1° × 1°) grids. The MCS or non-MCS regions that are smaller than 16 0.25° grids were included when computing the domain Forg, but were excluded when computing the averaged ω_{500}. As the standard deviation of ω_{500} within each contribution can be over 0.3 Pa/s, we did not include the error bars in this figure.

4. LW ACRE and ω_{500} of MCS and Non-MCS

To find the dependence of LW ACRE or ω_{500} on the degree of convective organization, we sort the averages of LW ACRE and ω_{500} in the MCS and non-MCS regions into bins of every 10th percentile of a convective organization metric for each domain. Figure 2 shows the relationship between ω_{500} and the percentile of Forg over the 10° × 10° domains that are centered on the centroid of each MCS. For the MCS regions (shown as blue bars), the upward motion increases with Forg. The averaged ω_{500} in the 80%–100% Forg bin (>0.16 Pa/s) can reach more than 3 times larger than the one of the 0%–20% bin (~0.05 Pa/s). The ω_{500} results based on COP and Aorg (not shown) also exhibit an increase with the degree of organization, although the magnitude of the increase for COP is generally smaller than that for Forg and Aorg. For instance, the averaged ω_{500} in the 80%–100% COP bin is only 1.8 times larger than that in the 0%–20% COP bin. For Forg, the averaged ω_{500} over the non-MCS regions (shown as purple bars) is less than 0.05 Pa/s. Although the ω_{500} of non-MCS regions also increases with Forg, such an increase becomes insignificant (less than 0.02 Pa/s) for Forg from 40% to 100%. The degree of spatial organization of MCSs is, therefore, strongly linked to the vertical circulations between the MCS and non-MCS regions.

The MCS and non-MCS regions are further stratified into the heavy precipitation regions (grid points with precipitation rate larger than 2 mm/hr) and the light precipitation regions (grid points with precipitation rate equal to or smaller than 2 mm/hr). The threshold of 2 mm/hr corresponds to the 80th percentile of the mean MCS precipitation. The ω_{500} in these heavy precipitation regions outside MCSs (shown as green bars) is slightly smaller than the one in the heavy precipitation regions inside MCSs (shown as red bars). It is even larger than the averaged ω_{500} for all MCS regions (the blue bars). This means that the upward velocity of isolated deep convective storms and some small pockets of nimbostratus clouds outside MCSs can exceed the average of all MCSs. The ascent of the light precipitation regions outside MCSs (shown as cyan bars) is 3–5 times weaker than the counterparts inside MCSs (the yellow bars) as a result of the compensating downward and/or near-zero vertical motion in the regions between the MCSs. Overall, the differences of ω_{500} between MCS and non-MCS increase with the degree of organization (e.g., red bar vs. green bar in Figure 2).

How does the LW ACRE vary with the degree of convective organization and mean precipitation? Figure 3 shows the relationship between the LW ACRE and the percentile of Forg over the domains that are centered on the

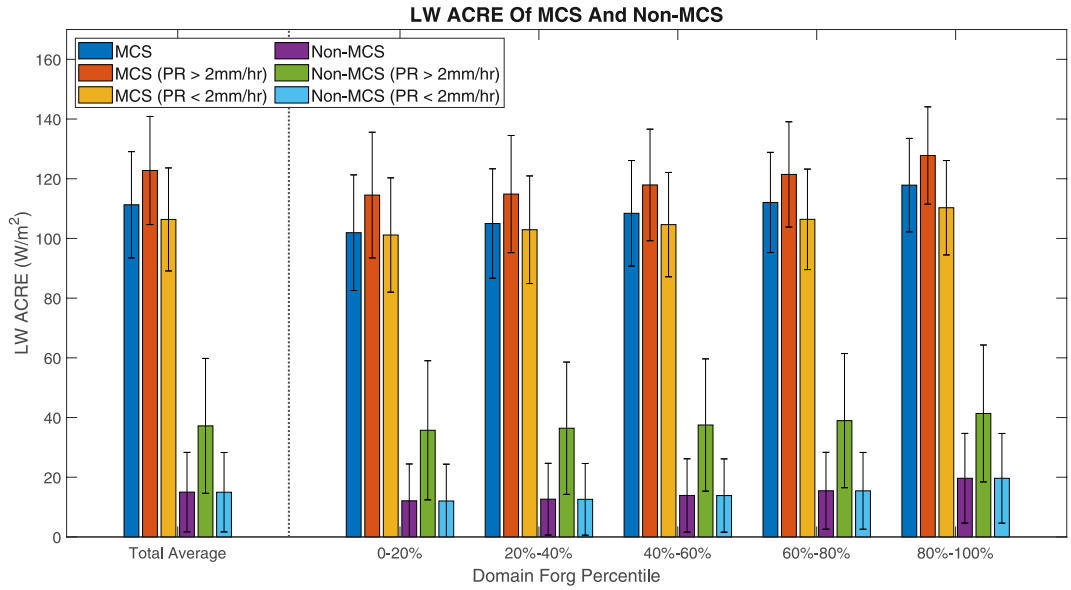

Figure 3. Averaged LW ACRE (w/m^2) as a function of the percentiles of Forg over 10° × 10° domains, divided into contributions as follows: MCS (blue), MCS with precipitation rate larger than 2 mm/hr (red), MCS with precipitation rate smaller than 2 mm/hr (yellow), non-MCS (purple), non-MCS with precipitation rate larger than 2 mm/hr (green), and non-MCS with precipitation smaller than 2 mm/hr (cyan). Each domain is centered on a centroid of an MCS larger than 16 0.25° grids. Error bars represent ± one standard deviation. The MCS or non-MCS regions that are smaller than 16 0.25° grids were included when computing the domain Forg percentile, but were excluded when computing the averaged LW ACRE.

centroid of each MCS. All different MCS regions have strongly enhanced LW ACRE (~110–130 W/m^2) relative to their non-MCS counterparts (~10–40 W/m^2). However, the MCSs over a strongly organized domain only have a slight enhancement of the LW ACRE to those over a weakly organized domain. The LW ACRE of 80%–100% Forg exhibits <20% more heating than of 0%–20% Forg. The relationship between LW ACRE and domain-mean precipitation (Figure S4 in Supporting Information S1) is very similar. The results based on COP and Aorg (not shown) also do not indicate any significant increase in heating from a less to more organized domain nor a weak to heavy precipitating one. This is different from the behavior of vertical velocity in Figure 2, in which the strength of the vertical motions is tightly linked to the degree of organization and mean precipitation.

The primary finding in Figure 3 is that the LW ACRE is much larger in the MCS regions than in the non-MCS regions (greater than 5 times). Even though the LW ACRE of the non-MCS regions of heavy precipitation (green bars) is twice as large as that of the non-MCS regions of light precipitation (cyan bars), it is still about 3 times smaller than the heating of the MCS regions (red and orange bars). The differences in LW ACRE between MCS and non-MCS regions (blue minus purple in Figure 3) are typically 98 W/m^2 and do not increase with the degree of organization. The ranges of LW ACRE variances, shown as one standard deviation error bars in Figure 3, also do not overlap between MCS and non-MCS regions. These findings are further supported by the results based on COP and Aorg for all three diagnoses and different sizes of domains (10° × 10°–30° × 30°).

5. Effects of Contrasting LW ACRE Between MCS and Non-MCS Regions on Individual MCSs and Convective Organization

Despite the weak connection between the LW ACRE and the degree of organization of MCSs, the large difference in LW ACRE between the MCS and non-MCS regions could still be important for the development of individual MCSs. Figure 4 exhibits the spatial composites of LW ACRE over the 10° × 10° domains centered on the centroid of the MCS composited for all MCSs from 2001 to 2017. The centered MCSs are sorted into four categories in terms of precipitation intensity, ranging from 0%–25% to 75%–100% of the mean MCS precipitation. Furthermore, the composites are constructed for each MCS category based on the lowest 30% (Figure 4 top row) and highest 30% (Figure 4 bottom row) of the Forg. Regardless of the spatial organization of MCSs over the domain, both the LW ACRE at the center and the size of MCS occurrence (Figure 4, orange and yellow shading) increase from category 1 to 4. According to Figure 4 ω_{500} contours, more developed MCSs exhibit a stronger ascent.

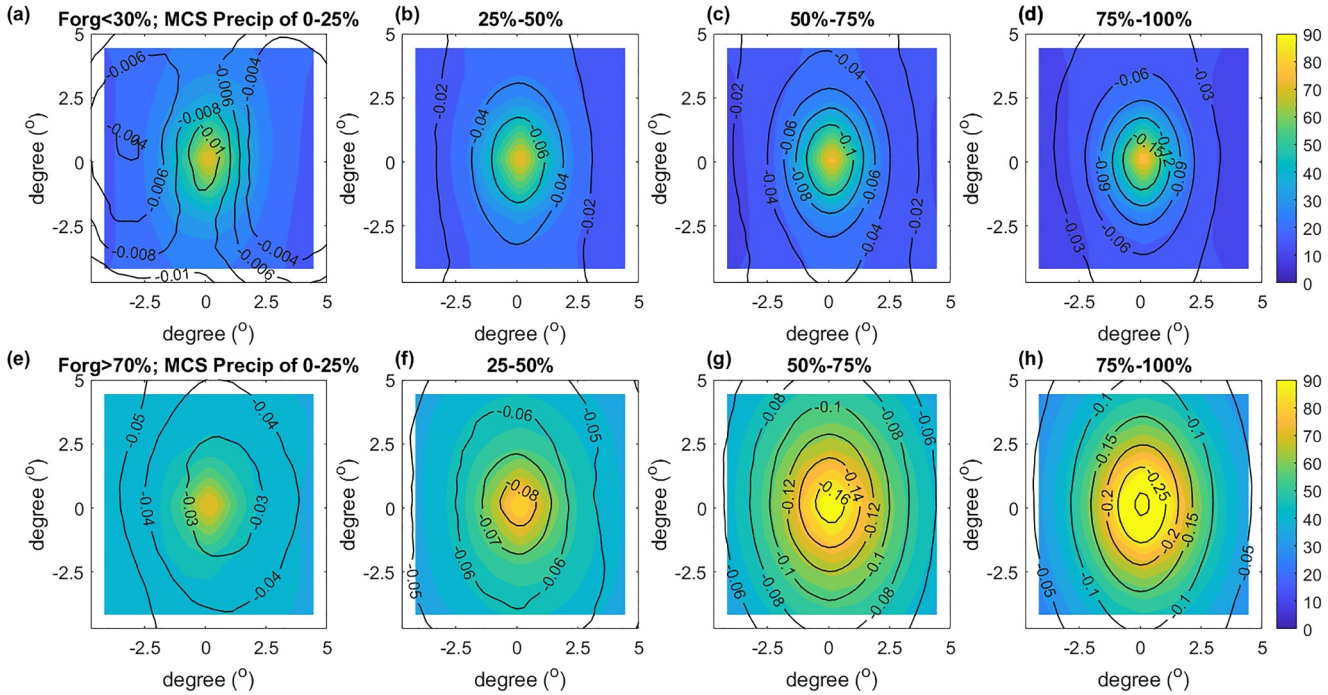

Figure 4. Spatial composites of LW ACRE (as shading) and ω_{500} (as black contours) of the 10° × 10° domains that are centered on the centroid of each MCS larger than 16 0.25° grids. The upper row shows the composites of the bottom 30% of Forg and the bottom one is for the average of the top 30% of Forg. The four columns indicate four precipitation categories of the centered MCS (larger than 16 0.25° grids): 0–25th percentile, 25–50th percentile, 50–75th percentile, and 75–100th percentile of the average precipitation of the centered MCS. Colors ranging from orange to yellow (i.e., LW ACRE >70 w/m^2) roughly correspond to the frequency of MCS (of all cases in each composite) ranging from 60% to 100%.

In Figure 5, MCSs in regions with a higher degree of organization show stronger upward vertical motion compared to regions with less organization. The difference in the vertical velocity is clear: in strongly organized cases (bottom row of Figure 5), the strongest upward motion occurs almost twice as intensely and at a higher altitude (in the upper troposphere, around 400 hPa) than in weakly organized cases (top row), where it peaks at a lower altitude (around 750 hPa). In addition, the strength of MCS-averaged precipitation increases with the degree of organization measured by Forg, Aorg, and COP (e.g., Figure S1 in Supporting Information S1). Overall, these indicate that a higher degree of convective organization corresponds to stronger vertical circulations inside and outside MCSs, stronger low-level convergence due to conservation of mass, and thus more developed MCSs.

Figure 4 also seems to suggest that the LW ACRE is related to the degree of convective organization, with highly organized cases showing twice as strong LW ACRE compared to the less organized ones. However, when focusing on the mean LW ACRE of individual MCSs, the difference is much smaller: the mean LW ACRE for strongly organized cases is only about 8–14 W/m2 (<8–14%) greater than for the weakly organized cases (as seen in Table 1, row 11 minus row 8). This increase is small compared to the much larger 30%–300% rise in ω_{500} (Table 1, row 2 vs. row 5). These findings suggest that the LW ACRE in MCSs is not very dependent on the degree of organization.

Another interesting finding from Table 1 is the consistent difference of LW ACRE between inside and outside an MCS (~70–80 W/m^2), regardless of the MCS category or degree of organization. This LW ACRE gradient is about 22%–25% of the average MSE import (~315 W/m^2) into the MCSs of the South Asia Summer Monsoon (Chen et al., 2021). This indicates that, as long as an MCS exists, the cloud-related radiative heating difference between the MCS and its surroundings could contribute to about a quarter of the MSE convergence, which is substantial for supporting individual MCSs.

To further inspect the relationship between convective organization and the contrast of LW ACRE (or ω_{500}) between MCS and non-MCS, we show ω_{500} (upper row) and LW ACRE (lower row) as a joint function of both the degree of organization and mean precipitation over the domains in Figure 6. These relationships are illustrated as colored tile grids for MCS, non-MCS, and the differences between MCS and non-MCS. Across the three domain

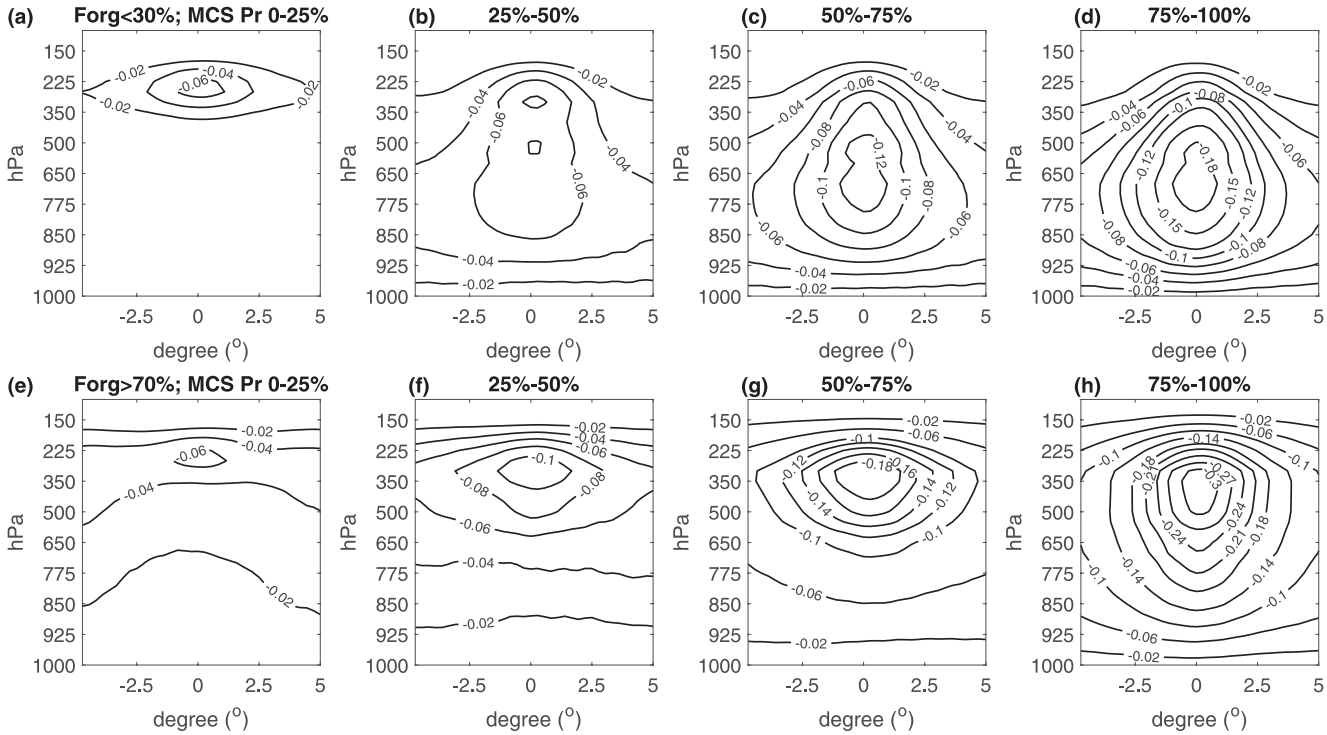

Figure 5. Composites of vertical velocity at 1,000 to 100 hPa of the 10° × 10° domains that are centered on the centroid of each MCS larger than 16 0.25° grids. The arrangement of the plots (by percentile ranges of the average precipitation of the centered MCS) is in the same order as in Figure 4.

selection approaches and three convective organization metrics (Forg, Aorg, and COP), the ω_{500} primarily depends on domain-averaged precipitation rather than the degree of organization. For a given domain-mean precipitation percentile bin, the ω_{500} generally increases with the degree of organization before decreasing for MCS (Figure 6a), non-MCS (Figures 6b and 6c), and the difference between MCS and the drier part of non-MCS (Figure 6d). The only exception is in the 90%–100% domain-mean precipitation bin for MCS (Figure 6a), where the ω_{500} increases with the degree of organization from the 0%–10% to 90%–100% bins.

Table 1
Mean ω_{500} (Unit: Pa/s) and LW ACRE (Unit: W/m^2) of the Centered MCS in Figure 4 and of the Regions Outside the Centered MCS (Include Both Non-MCSs and Other MCSs) for the Four MCS Categories

	Category 1 (0%–25% MSC precipitation)	Category 2 (25%–50%)	Category 3 (50%–75%)	Category 4 (75%–100%)
ω inside MCS (<30%)	−0.083 ± 0.118	−0.523 ± 0.171	−0.844 ± 0.205	−1.447 ± 0.262
ω outside MCS (<30%)	−0.040 ± 0.045	−0.180 ± 0.048	−0.248 ± 0.052	−0.375 ± 0.058
Δω (<30%)	−0.043 ± 0.109	−0.343 ± 0.163	−0.596 ± 0.197	−1.072 ± 0.254
ω inside MCS (>70%)	−0.268 ± 0.142	−0.682 ± 0.150	−1.018 ± 0.154	−1.898 ± 0.200
ω of outside MCS (>70%)	−0.383 ± 0.064	−0.459 ± 0.063	−0.495 ± 0.066	−0.616 ± 0.074
Δω (>70%)	0.115 ± 0.136	0.223 ± 0.143	−0.523 ± 0.147	−1.282 ± 0.197
ACRE inside MCS (<30%)	100.83 ± 19.65	102.81 ± 18.73	104.82 ± 19.37	106.42 ± 20.48
ACRE outside MCS (<30%)	33.36 ± 15.41	29.85 ± 15.58	28.03 ± 15.80	26.80 ± 16.46
ΔACRE (<30%)	67.47 ± 22.04	72.96 ± 22.51	76.78 ± 22.89	79.62 ± 23.40
ACRE inside MCS (>70%)	112.38 ± 20.64	111.12 ± 19.56	114.01 ± 17.32	120.14 ± 16.82
ACRE outside MCS (>70%)	41.30 ± 16.87	42.82 ± 19.03	46.36 ± 20.50	43.70 ± 21.61
ΔACRE (>70%)	71.08 ± 25.64	68.30 ± 26.85	67.65 ± 25.60	76.44 ± 25.24

Note. <30% (>70%) in parentheses represents the cases of Forg <30% (>70%). Δ stands for inside MCS minus outside MCS. Values after the "±" sign represent one standard deviation.

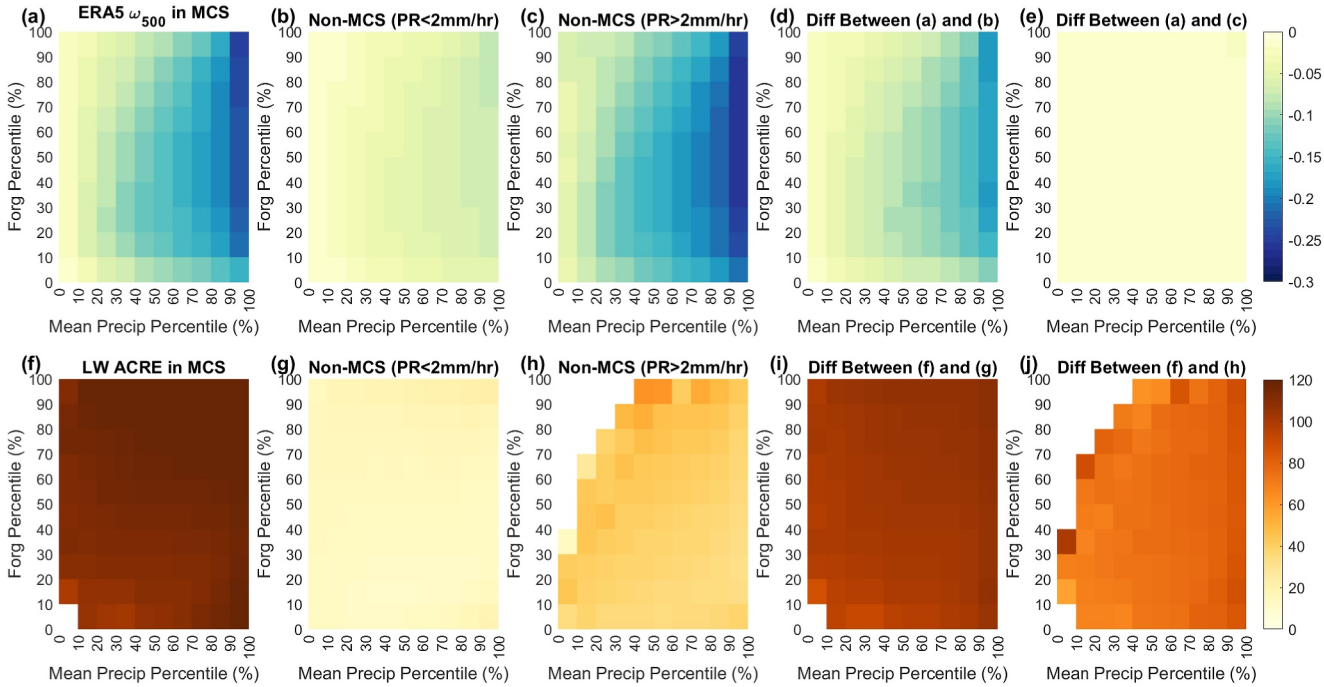

Figure 6. Averaged hourly ω_{500} (Pa/s; upper, blue) and LW ACRE (W/m^2; lower, orange) as a joint function of Forg percentiles (*y*-axis) and percentiles of domain mean precipitation (*x*-axis) for MCS (a and f), non-MCS with precipitation smaller than 2 mm/hr (b and g), non-MCS with precipitation larger than 2 mm/hr (c and h), and the differences between MCS and the two non-MCS regions. Each domain is based on 10° × 10° domains centered on a centroid of an MCS larger than 16 0.25° grids. The MCS or non-MCS regions that are smaller than 16 0.25° grids were included when computing the domain Forg and precipitation, but were excluded when computing the averaged ω_{500} and LW ACRE.

Unlike the difference of ω_{500} between MCS and non-MCS, the difference of LW ACRE between MCS and non-MCS; however, does not exhibit an increase with both mean precipitation and spatial organization of MCSs. The enhancement of ACRE difference between MCS and non-MCS from 0%–20% to 80%–100% of the degree of organization (for a certain mean precipitation) is generally 0–10 W/m^2 for Forg, 0–5 W/m^2 for COP, and ∼0 W/m^2 for Aorg. Therefore, it is unlikely that the convective organization of MCSs measured by Forg, Aorg, and COP is strongly associated with the contrast of LW ACRE between MCS and non-MCS. Instead, the degree of organization here, unlike the convective aggregation indices used in RCE studies, appears to be more closely linked to domain-mean precipitation, which is, in turn, highly correlated with the mean mid-level vertical ascent (e.g., Figure S3 in Supporting Information S1) and low-level convergence.

6. Temporal Evolution of the Relationships Among Convective Organization and LW ACRE and ω_{500}

In this section, we seek to understand whether the relationships between the spatial organization of MCSs and LW ACRE/ω_{500} change over time. For each spatial-averaging domain, we collect the domain degree of organization as well as MCS- and non-MCS-related LW ACRE and ω_{500} every 3 hr from the 12 hr before the occurrence of the reference MCSs at Hour 0 to the 12 hr after. Note that at other hours there could be different MCSs within a given 10° by 10° analysis subdomain; since an average MCS lifetime is roughly 12 hr (Huang et al., 2018), toward the ends of the ±12 hr window, the estimate should be interpreted as relevant for MCSs in the domain rather than the reference MCSs.

Figure 7 shows the temporal evolution of the relationship between the degree of organization and LW ACRE for this 24-hr window. Note that the MCS evolution in this plot is a statistical evolution of MCSs within a region, not a tracking of an individual MCS. The changes of LW ACRE are very moderate for any degree of organization during the entire period: <15 W/m^2 for the MCS regions and <5 W/m^2 for the non-MCS ones. The difference in LW ACRE between MCS and non-MCS remains relatively constant before and after the MCS, typically about 90–100 W/m^2. An overview statement of this result is that the LW ACRE difference between MCS and non-MCS

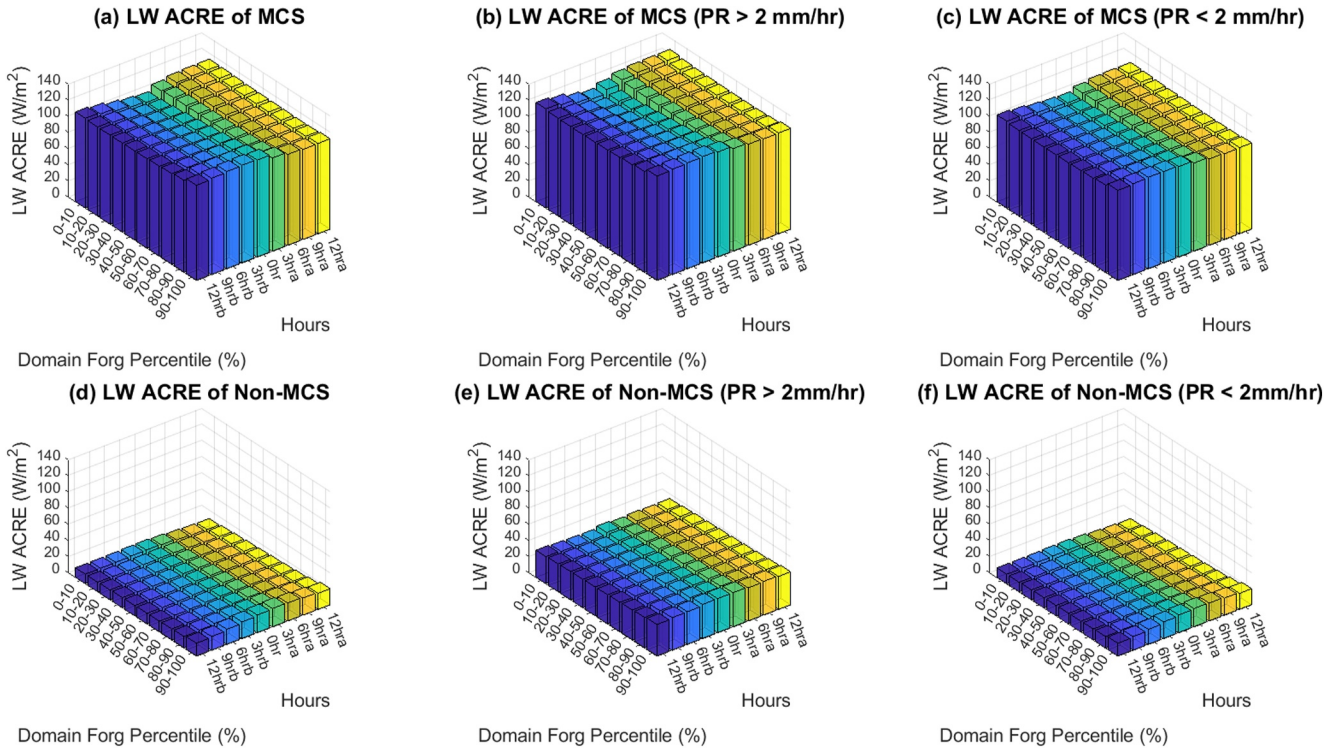

Figure 7. Temporal evolution of LW ACRE (averaged over each 10° × 10° domain; *z*-axis) as a function of Forg percentile (*y*-axis) in that domain, divided into contributions as follows: (a) within MCS; (b) within MCS for grid points with precipitation rate greater than 2 mm/hr; (c) within MCS for grid points with precipitation rate smaller than 2 mm/hr; (d) within non-MCS; (e) within non-MCS for grid points with precipitation rate greater than 2 mm/hr; (f) within non-MCS for grid points with precipitation rate smaller than 2 mm/hr. The *x*-axis shows 12 to 3 hr before the MCS hour (0 hr) and 3–12 hr after the MCS hour. Different colors represent different hours. Each domain is a 10° × 10° one centered on a centroid of an MCS larger than 16 0.25° grids. At each hour, the MCS or non-MCS regions that are smaller than 16 0.25° grids were included when computing domain Forg, but were excluded when computing averaged ω_{500}.

doesn't change much with convective organization or during MCS evolution. We postulate that a straightforward explanation for this is: For individual MCSs, once the stratiform/anvil cloud associated with the MCS is established (typically with a cloud-top height greater than 10 km for >86% of all MCSs, Yuan et al., 2011), the radiative effect per unit area does not change much as the area of the MCS increases. If the cloud-top temperature of the stratiform area tends to change with the spatial organization of MCSs, one would see the effects, but the result here suggests that the cloud-top temperature (and emissivity) is not changing strongly in time or with convective organization. An implication is that the rate of feedback favors the growth of individual MCSs to a similar extent throughout the lifecycle and without strong dependence on the presence or absence of other MCSs in the region.

Similar to Figures 7, Figure 8 presents the temporal evolution of the relationship between the degree of organization and ω_{500}. We note that the ERA5 reanalyzed vertical velocity may not be accurate (e.g., Serra et al., 2023) although ERA5 has successfully been used for the analysis of MCS associations (Hsu et al., 2023; Serra et al., 2023)—we aim here for overall statistical relations regarding the association with MCS. If ongoing convective organization of MCSs or the MCS development causes the negative vertical velocity at a large scale, we would expect the upward motion inside MCSs to keep increasing until the MCS occurrence (Hour 0 in Figure 8). However, for stronger spatial organization of MCSs, the temporal evolution in Figure 8 suggests that the upward motion in the MCS environment (Figures 8a–8c) is favorable for the development of MCSs at the earlier stages (12–3 hr before the MCS) and becomes weaker during Hour 0 and afterward. For weakly organized cases, the MCS relationship to vertical velocity is even less consistent with MCS development having a causal effect on vertical velocity. A similar dependence of ω_{500} on time and degree of organization can be found inside and outside the MCSs. Therefore, the modest amplitude but more negative values of ω_{500} associated with stronger organization of MCSs suggest that large-scale low-level convergence (here estimated over each 10° × 10° or larger subdomain in the analysis) is a likely factor in increasing the organization of the MCSs, and not vice versa.

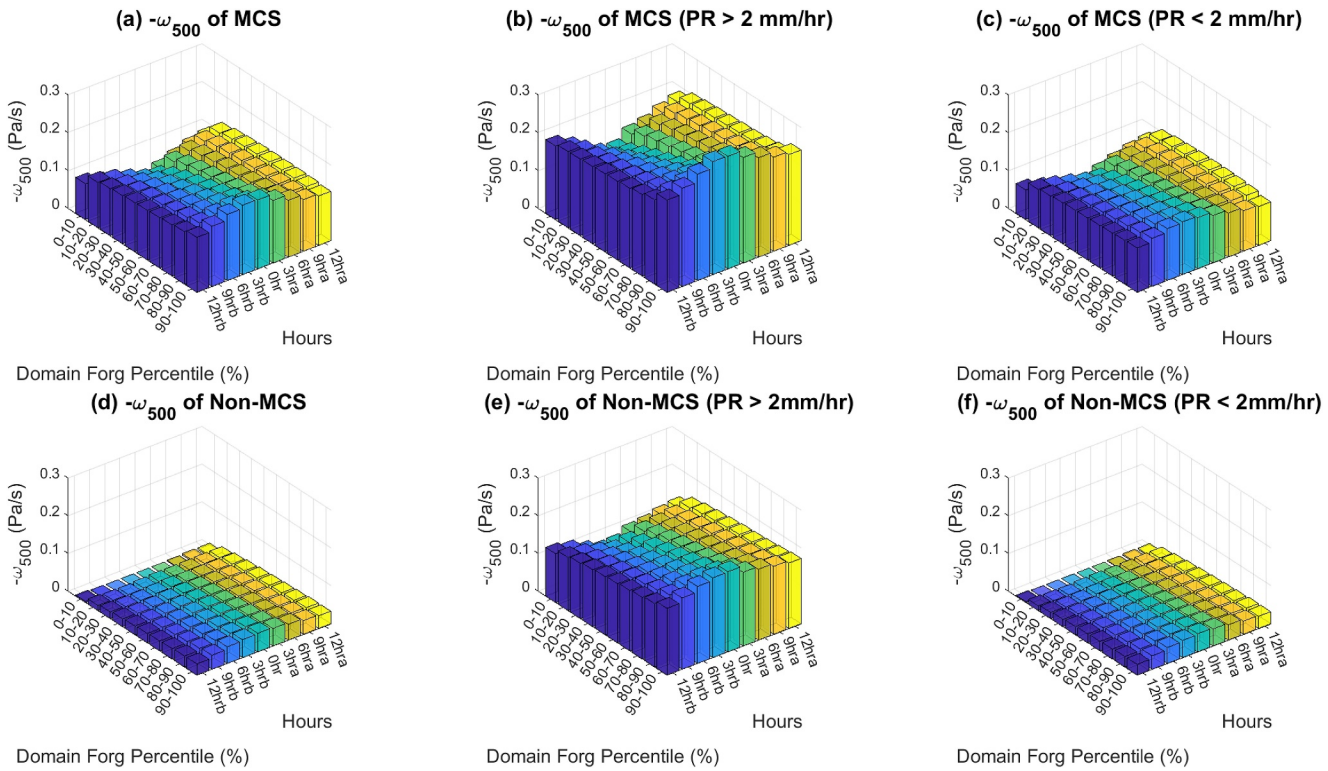

Figure 8. Temporal evolution of $-\omega_{500}$ (averaged over each 10° × 10° domain; *z*-axis) as a function of Forg percentile (*y*-axis) in that domain, divided into contributions as follows: (a) within MCS; (b) within MCS for grid points with precipitation rate greater than 2 mm/hr; (c) within MCS for grid points with precipitation rate smaller than 2 mm/hr; (d) within non-MCS; (e) within non-MCS for grid points with precipitation rate greater than 2 mm/hr; (f) within non-MCS for grid points with precipitation rate smaller than 2 mm/hr. The *x*-axis shows 12 to 3 hr before the MCS hour (0 hr) and 3–12 hr after the MCS hour. Different colors represent different hours. Each domain is a 10° × 10° one centered on a centroid of an MCS larger than 16 0.25° grids. At each hour, the MCS or non-MCS regions that are smaller than 16 0.25° grids were included when computing domain Forg, but were excluded when computing averaged LW ACRE.

The non-MCS regions also experience large-scale convergence, which would favor more spatial organization of MCSs. This is consistent with the larger vertical velocity even in non-MCS raining parts of the region (Figure 8e) for strongly organized cases.

The real atmosphere is not at the strict radiative-convective equilibrium, especially locally (if it were, the increase in ACRE could limit precipitation). However, the balance between radiative cooling and convective heating tends to only be reached on larger scales (e.g., several thousand kilometers; Tomassini, 2020). The large-scale convergence appears to be the leading order effect in the convective organization of MCSs on a smaller scale domain (e.g., 10° × 10°–30° × 30°). Although the LW ACRE favors rising motion in individual MCSs, apparently it is not the dominant factor for developing more mesoscale convective organization as in the RCE simulations. Again, our convective organization metrics are strongly associated with domain-mean precipitation, unlike the convective aggregation indices used for RCE studies.

7. Conclusions

The effect of cloud radiative heating and cloud-radiation feedback on tropical convection and circulations has been one of the popular topics in theory and modeling studies. In this study, we seek the observed relationships between the column cloud radiative heating and the spatial organization of tropical MCSs during the period of 2001–2017. We compare six convective organization metrics, including two newly defined metrics (Forg and Aorg) that characterize the intensity of interactive MCSs over a domain. Three of these, Iorg, AOS, and σCWV, do not exhibit sufficiently clear relationships to the domain-averaged MCS area. COP, Forg, and Aorg are chosen as the main three organization metrics for this study as the degree of organization indicated by these three metrics is positively related to the horizontal size of the MCS organization.

We find that the LW ACRE is important for maintaining individual MCSs. The LW ACRE of MCS and non-MCS, as well as the difference in LW ACRE between the MCS and non-MCS, are relatively constant during the life cycle of MCSs, regardless of the degree of organization and domain-mean precipitation. In other words, the radiative feedback favors the growth or maintenance of individual MCS to a similar extent throughout the lifecycle and without strong dependence on the regional degree of organization. The contrast of LW ACRE between MCS and non-MCS is about 90–100 W/m^2. For reference, this is more than a quarter of a typical MSE import into the South Asian Summer Monsoon (e.g., Chen et al., 2021). Several recent studies (e.g., Ruppert et al., 2020; Wu et al., 2021) have also highlighted the significance of LW ACRE and radiative feedback in tropical cyclone development, both in observations and models. These studies demonstrated that LW radiative feedback can play a crucial role in influencing mesoscale and synoptic-scale circulations over timescales of days.

We carefully examine the role played by LW ACRE on the spatial organization of MCSs over domains ranging from 10° × 10°–30° × 30°, including conducting three different diagnoses using different selections of the domains, comparing different convective organization metrics, and dissecting the relationship between LW ACRE and the degree of organization in terms of heavy precipitating (>2 mm/hr) and light precipitation (<2 mm/hr) regions of MCS and non-MCS. However, the LW ACRE for MCS, non-MCS, and their differences are not strongly linked to the observed spatial organization of MCSs or domain mean precipitation on this horizontal scale.

Instead, we find that there is a robust dependence between the degree of organization and upward motion in the very large-scale environment (domains ranging from 10° × 10°–30° × 30° in this study), that is, not the environment of an individual MCS but that of multiple MCSs whose spatial organization is being estimated. The mean ω_{500} in both the MCS and non-MCS regions scales with the domain-mean precipitation (Figure S3 in Supporting Information S1). The strongly organized cases tend to have larger vertical velocity in MCSs as well as in the non-MCS raining parts of the domain, and the time evolution is consistent with the large-scale low-level convergence being forced by outside factors rather than being purely internally determined by the MCSs in the domain. In particular, large-scale low-level convergence is associated with the enhancement of mesoscale organization of convection in the earlier stages of MCS development. The effect of observed large-scale convergence on the mesoscale convective organization thus appears to be the first-order effect in realistic atmospheric conditions, an effect that is often omitted or simplified in organization studies conducted in radiative-convective equilibrium. Although the contrast of radiative heating between MCS and non-MCS is seen as important within each MCS, in these results, it is secondary to the spatial organization of MCSs.

Modeling studies in which large-scale convergence is important to the convective organization include a cloud-resolving modeling study with imposed vertical velocity (Su et al., 2000) and intermediate complexity modeling with imposed stochastic circulation (Ahmed et al., 2021). Bretherton and Khairoutdinov (2015) used a near-global aquaplanet cloud-resolving model and found that, on a global scale, the positive cloud-radiative feedback on self-aggregation tends to be balanced out by the negative surface-flux feedback on the MSE import due to the global-scale circulations ultimately driven by SST gradients. These feedback typically unfold around 10 days in the model, which is significantly longer than the duration of interaction between convection and large-scale circulations. Hence, they argued that radiative feedback is likely only important for global-scale tropical circulations. An observation analysis within the gross moist stability framework by Tsai and Mapes (2022) revealed a balance between radiative cooling and surface flux during the process of convective aggregation in areas of 5° × 5° over a 4-day time window. Arnold and Putman (2018) found that large-scale low-level flow is the root cause of the upper size limit (around 4,000 km) of aggregated convective clusters in nonrotating simulations in an atmospheric GCM with uniform SSTs. Yang (2018b) successfully predicted the wavelength of convective self-aggregation and its association with SSTs using 2D CRM simulations imposed with steady large-scale circulations (∼10,000 km). In his work, the horizontal pressure and buoyancy gradients in the boundary layer were essential for maintaining the large-scale circulations associated with self-aggregation. Our observational work supports these model results, highlighting the importance of large-scale circulations on the development of mesoscale convective organization.

One caveat of this study is that the horizontal resolution of the hourly CERES fluxes is 1° × 1°, which is 16 times coarser than the one of the IMERG precipitation and the masks of MCS and/or non-MCS. In this study, we excluded the MCSs smaller than a 1° grid box. However, including these small-sized MCSs in the calculations yielded very similar results (e.g., Figures S5 and S6 in Supporting Information S1 compared to Figures 2 and 3),

suggesting that the coarse resolution of CERES data does not compromise the robustness of our findings. The vertical velocity used in this study is from the ERA5 reanalysis. Although ERA5 reanalysis provides hourly vertical velocity estimates with extensive global coverage, these estimates of vertical velocity have large variances in both the MCS and non-MCS regions and can exhibit large biases when compared to the actual vertical wind measurements (e.g., Serra et al., 2023). Future research on MCSs and convective organization would benefit from high-resolution observations and quantitative measurements of radiative fluxes, rainfall, and wind profiles, especially with finer temporal, horizontal, and vertical resolutions.

Data Availability Statement

The CERES SYN1deg-1Hour fluxes (Doelling et al., 2016) used for calculating the LW ACRE in this study were obtained from the NASA Langley Research Center Atmospheric Science Data Center via 10.5067/Terra+Aqua/CERES/SYN1deg-1Hour_L3.004 (NASA/LARC/SD/ASDC, 2017). The hourly vertical velocity from the ECMWF ERA5 reanalysis (Hersbach et al., 2020) is available in the ECMWF Copernicus Climate Data Store via 10.24381/cds.bd0915c6 (Hersbach et al., 2023a). The hourly column water vapor from the ERA5 reanalysis is available in the ECMWF Copernicus Climate Data Store via 10.24381/cds.adbb2d47 (Hersbach et al., 2023b). The half-hourly IMERG precipitation data were provided by the NASA/Goddard Space Flight Center's Precipitation Measurement Missions Science Team and PPS, which developed and computed the IMERG as a contribution to the GPM project and are archived at the NASA GES DISC via 10.5067/GPM/IMERG/3B-HH/07 (Huffman et al., 2014). The GPM_MERGIR brightness temperature data used for computing the MCS masks are also available at NASA GES DISC via 10.5067/P4HZB9N27EKU (Janowiak et al., 2017). Data analysis and visualization were done with MATLAB version R2023b (The MathWorks Inc, 2023), which is preserved at https://www.mathworks.com/products/new_products/release2023b.html, and the MATLAB scripts are available at 10.5281/zenodo.14053496 (Dai, 2024).

Acknowledgments

This work was supported by the U.S. Department of Energy's Regional & Global Model Analysis (DOE-RGMA) program under Award DE-SC0021312, the National Oceanic and Atmospheric Administration's Modeling, Analysis, Predictions, and Projections (NOAA-MAPP) program under Award NA20OAR4310394, and the National Science Foundation (NSF) under Award AGS-2414576. HS acknowledges the funding support from the Hong Kong Jockey Club Charities Trust (FA123) and RGC General Research Fund (16300823 and 16308924). We sincerely thank Dr. Blaž Gasparini and the three anonymous reviewers for their in-depth review and valuable comments, which greatly improved this manuscript.

References

Ahmed, F., Neelin, J. D., & Adames, Á. F. (2021). Quasi-equilibrium and weak temperature gradient balances in an equatorial beta-plane model. *Journal of the Atmospheric Sciences*, *78*(1), 209–227. https://doi.org/10.1175/JAS-D-20-0184.1

Albern, N., Voigt, A., Buehler, S. A., & Grützun, V. (2018). Robust and nonrobust impacts of atmospheric cloud-radiative interactions on the tropical circulation and its response to surface warming. *Geophysical Research Letters*, *45*(16), 8577–8585. https://doi.org/10.1029/2018GL079599

Angulo-Umana, P., & Kim, D. (2023). Mesoscale convective clustering enhances tropical precipitation. *Science Advances*, *9*(2), eabo5317. https://doi.org/10.1126/sciadv.abo5317

Arnold, N. P., & Putman, W. M. (2018). Nonrotating convective self-aggregation in a limited area AGCM. *Journal of Advances in Modeling Earth Systems*, *10*, 1029–1046. https://doi.org/10.1002/2017MS001218

Benedict, J. J., Medeiros, B., Clement, A. C., & Olson, J. (2020). Investigating the role of cloud-radiation interactions in subseasonal tropical disturbances. *Geophysical Research Letters*, *47*(9), e2019GL086817. https://doi.org/10.1029/2019GL086817

Bony, S., Semie, A., Kramer, R. J., Soden, B., Tompkins, A. M., & Emanuel, K. A. (2020). Observed modulation of the tropical radiation budget by deep convective organization and lower-tropospheric stability. *AGU Advances*, *1*(3), e2019AV000155. https://doi.org/10.1029/2019AV000155

Bretherton, C. S., Blossey, P. N., & Khairoutdinov, M. (2005). An energy-balance analysis of deep convective self-aggregation above uniform SST. *Journal of the Atmospheric Sciences*, *62*(12), 4273–4292. https://doi.org/10.1175/JAS3614.1

Bretherton, C. S., & Khairoutdinov, M. F. (2015). Convective self-aggregation feedbacks in near-global cloud-resolving simulations of an aquaplanet. *Journal of Advances in Modeling Earth Systems*, *7*(4), 1765–1787. https://doi.org/10.1002/2015MS000499

Cess, R. D., Potter, G. L., Blanchet, J. P., Boer, G. J., del Genio, A. D., Déqué, M., et al. (1990). Intercomparison and interpretation of climate feedback processes in 19 atmospheric general circulation models. *Journal of Geophysical Research*, *95*(D10), 16601–16615. https://doi.org/10.1029/JD095iD10p16601

Chen, X., Leung, L. R., Feng, Z., Song, F., & Yang, Q. (2021). Mesoscale convective systems dominate the energetics of the South Asian summer monsoon onset. *Geophysical Research Letters*, *48*(17), e2021GL094873. https://doi.org/10.1029/2021GL094873

Chou, C., Chen, C., Tan, P., & Chen, K. T. (2012). Mechanisms for global warming impacts on precipitation frequency and intensity. *Journal of Climate*, *25*(9), 3291–3306. https://doi.org/10.1175/JCLI-D-11-00239.1

Dai, N. (2024). niiidai/Dai_etal_ACRE_MCS_2024: November 07, 2024 release (version 1.0.0.0-alpha) [Software]. *Zenodo*. https://doi.org/10.5281/zenodo.14053495

Dai, N., Kramer, R. J., Soden, B. J., & L'Ecuyer, T. S. (2021). Evaluation of CloudSat radiative kernels using ARM and CERES observations and ERA5 reanalysis. *Journal of Geophysical Research: Atmospheres*, *126*(23), e2020JD034510. https://doi.org/10.1029/2020JD034510

Dai, N., & Soden, B. J. (2020). Convective aggregation and the amplification of tropical precipitation extremes. *AGU Advances*, *2*(4), e2020AV000201. https://doi.org/10.1029/2020AV000201

Dee, D. P., Uppala, S. M., Simmons, A. J., Berrisford, P., Poli, P., Kobayashi, S., et al. (2011). The ERA-interim reanalysis: Configuration and performance of the data assimilation system. *Quarterly Journal of the Royal Meteorological Society*, *137*(656), 553–597. https://doi.org/10.1002/qj.828

Doelling, D. R., Sun, M., Nguyen, L. T., Nordeen, M. L., Haney, C. O., Keyes, D. F., & Mlynczak, P. E. (2016). Advances in geostationary-derived longwave fluxes for the CERES synoptic (SYN1deg) product. *Journal of Atmospheric and Oceanic Technology*, *33*(3), 503–521. https://doi.org/10.1175/JTECH-D-15-0147.1

Emanuel, K. A. (2007). Quasi-equilibrium dynamics of the tropical atmosphere. In T. Schneider & A. H. Sobel (Eds.), *The global circulation of the atmosphere* (pp. 186–218). Princeton University Press.

Emanuel, K. A., David Neelin, J., & Bretherton, C. S. (1994). On large-scale circulations in convecting atmospheres. *Quarterly Journal of the Royal Meteorological Society*, *120*(519), 1111–1143. https://doi.org/10.1002/qj.49712051902

Emori, S., & Brown, S. J. (2005). Dynamic and thermodynamic changes in mean and extreme precipitation under changed climate. *Geophysical Research Letters*, *32*(17), L17706. https://doi.org/10.1029/2005GL023272

Feng, Z., Hagos, S., Rowe, A. K., Burleyson, C. D., Martini, M. N., & de Szoeke, S. P. (2015). Mechanisms of convective cloud organization by cold pools over tropical warm ocean during the AMIE/DYNAMO field campaign. *Journal of Advances in Modeling Earth Systems*, *7*(2), 357–381. https://doi.org/10.1002/2014MS000384

Feng, Z., Houze, R. A., Leung, L. R., Song, F., Hardin, J. C., Wang, J., et al. (2019). Spatiotemporal characteristics and large-scale environments of mesoscale convective systems east of the Rocky Mountains. *Journal of Climate*, *32*(21), 7303–7328. https://doi.org/10.1175/JCLI-D-19-0137.1

Harrop, B. E., & Hartmann, D. L. (2016). The role of cloud radiative heating within the atmosphere on the high cloud amount and top-of-atmosphere cloud radiative effect. *Journal of Advances in Modeling Earth Systems*, *8*(3), 1391–1410. https://doi.org/10.1002/2016MS000670

Hazra, R., Park, S., Smith, G. L., & Reichenbach, S. E. (1993). Constrained least-squares image restoration filters for sampled image data. In A. Tescher (Ed.) *Applications of digital image processing XVI*. (Vol. 2028, pp. 177–192). SPIE.

Held, I. M., Hemler, R. S., & Ramaswamy, V. (1993). Radiative-convective equilibrium with explicit two-dimensional moist convection. *Journal of the Atmospheric Sciences*, *50*(23), 3909–3927. https://doi.org/10.1175/1520-0469(1993)050<3909:RCEWET>2.0.CO;2

Hersbach, H., Bell, B., Berrisford, P., Biavati, G., Horányi, A., Muñoz Sabater, J., et al. (2023a). ERA5 hourly data on pressure levels from 1940 to present [Dataset]. *Copernicus Climate Change Service (C3S) Climate Data Store (CDS)*. https://doi.org/10.24381/cds.bd0915c6

Hersbach, H., Bell, B., Berrisford, P., Biavati, G., Horányi, A., Muñoz Sabater, J., et al. (2023b). ERA5 hourly data on single levels from 1940 to present [Dataset]. *Copernicus Climate Change Service (C3S) Climate Data Store (CDS)*. https://doi.org/10.24381/cds.adbb2d47

Hersbach, H., Bell, B., Berrisford, P., Hirahara, S., Horányi, A., Muñoz-Sabater, J., et al. (2020). The ERA5 global reanalysis. *Quarterly Journal of the Royal Meteorological Society*, *146*(730), 1999–2049. https://doi.org/10.1002/qj.3803

Holloway, C. E., Wing, A. A., Bony, S., Muller, C., Masunaga, H., L'Ecuyer, T. S., et al. (2017). Observing convective aggregation. *Surveys in Geophysics*, *38*(6), 1199–1236. https://doi.org/10.1007/s10712-017-9419-1

Houze, R. A. Jr. (1989). Observed structure of mesoscale convective systems and implications for large-scale heating. *Quarterly Journal of the Royal Meteorological Society*, *115*(487), 425–461. https://doi.org/10.1002/qj.49711548702

Hsu, W.-C., Kooperman, G. J., Hannah, W. M., Reed, K. A., Akinsanola, A. A., & Pendergrass, A. G. (2023). Evaluating mesoscale convective systems over the US in conventional and multiscale modeling framework configurations of E3SMv1. *Journal of Geophysical Research: Atmospheres*, *128*(23), e2023JD038740. https://doi.org/10.1029/2023JD038740

Huang, X., Hu, C., Huang, X., Chu, Y., Tseng, Y. h., Zhang, G. J., & Lin, Y. (2018). A long-term tropical mesoscale convective systems dataset based on a novel objective automatic tracking algorithm. *Climate Dynamics*, *51*(7–8), 3145–3159. https://doi.org/10.1007/s00382-018-4071-0

Huffman, G., Bolvin, D., Braithwaite, D., Hsu, K., Joyce, R., & Xie, P. (2014). Integrated multi-satellitE retrievals for GPM (IMERG), version 4.4 [Dataset]. *NASA's Precipitation Processing Center*. https://doi.org/10.5067/GPM/IMERG/3B-HH/07

Janowiak, J., Joyce, B., & Xie, P. (2017). NCEP/CPC L3 half hourly 4km global (60S - 60N) merged IR V1 [Dataset]. In A. Savtchenko (Ed.) *Goddard Earth sciences data and information services center (GES DISC)*. https://doi.org/10.5067/P4HZB9N27EKU

Joyce, R., Janowiak, J., & Huffman, G. (2001). Latitudinally and seasonally dependent zenith-angle corrections for geostationary satellite IR brightness temperatures. *Journal of Applied Meteorology and Climatology*, *40*(4), 689–703. https://doi.org/10.1175/1520-0450(2001)040<0689:LASDZA>2.0.CO;2

Machado, L. A. T., & Rossow, W. B. (1993). Structural characteristics and radiative properties of tropical cloud clusters. *Monthly Weather Review*, *121*(12), 3234–3260. https://doi.org/10.1175/1520-0493(1993)121<3234:scarpo>2.0.co;2

Miller, R. A., & Frank, W. M. (1993). Radiative forcing of simulated tropical cloud clusters. *Monthly Weather Review*, *121*, 482–498. https://doi.org/10.1175/1520-0493(1993)121,0482:RFOSTC.2.0.CO;2

Minnis, P., Sun-Mack, S., Chen, Y., Chang, F. L., Yost, C. R., Smith, W. L., et al. (2021). CERES MODIS cloud product retrievals for edition 4—Part I: Algorithm changes. *IEEE Transactions on Geoscience and Remote Sensing*, *59*(4), 2744–2780. https://doi.org/10.1109/TGRS.2020.3008866

Minnis, P., Sun-Mack, S., Young, D. F., Heck, P. W., Garber, D. P., Chen, Y., et al. (2011). CERES edition-2 cloud property retrievals using TRMM VIRS and Terra and Aqua MODIS data-Part I: Algorithms. *IEEE Transactions on Geoscience and Remote Sensing*, *49*(11), 4374–4400. https://doi.org/10.1109/TGRS.2011.2144601

Muller, C. J., & Bony, S. (2015). What favors convective aggregation and why? *Geophysical Research Letters*, *42*(13), 5626–5634. https://doi.org/10.1002/2015gl064260

Muller, C. J., & Held, I. M. (2012). Detailed investigation of the self-aggregation of convection in cloud-resolving simulations. *Journal of the Atmospheric Sciences*, *69*(8), 2551–2565. https://doi.org/10.1175/jas-d-11-0257.1

Muller, C. J., Yang, D., George, C., Cronin, T., Benjamin, F., Haerter, J. O., et al. (2022). Spontaneous aggregation of convective storms. *Annual Review of Fluid Mechanics*, *54*(1), 133–157. https://doi.org/10.1146/annurev-fluid-022421-011319

NASA/LARC/SD/ASDC. (2017). CERES and GEO-enhanced TOA, within-atmosphere and surface fluxes, clouds and aerosols 1-hourly terra-aqua Edition4A SYN1deg-1hour [Dataset]. *NASA Langley Atmospheric Science Data Center DAAC*. https://doi.org/10.5067/TERRA+AQUA/CERES/SYN1DEG-1HOUR_L3.004A

Needham, M. R., & Randall, D. A. (2021). Linking atmospheric cloud radiative effects and tropical precipitation. *Geophysical Research Letters*, *48*(14), e2021GL094004. https://doi.org/10.1029/2021GL094004

O'Gorman, P. A., & Schneider, T. (2009). The physical basis for increases in precipitation extremes in simulations of 21st-century climate change. *Proceedings of the National Academy of Sciences of the United States of America*, *106*(35), 14773–14777. https://doi.org/10.1073/pnas.0907610106

Popp, M., & Silvers, L. G. (2017). Double and single ITCZs with and without clouds. *Journal of Climate*, *30*(22), 9147–9166. https://doi.org/10.1175/JCLI-D-17-0062.1

Ruppert, J. H., Jr., Wing, A. A., Tang, X., & Duran, E. L. (2020). The critical role of cloud–infrared radiation feedback in tropical cyclone development. *Proceedings of the National Academy of Sciences*, *117*(45), 27884–27892. https://doi.org/10.1073/pnas.2013584117

Schiro, K. A., Sullivan, S. C., Kuo, Y., Su, H., Gentine, P., Elsaesser, G. S., et al. (2020). Environmental controls on tropical mesoscale convective system precipitation intensity. *Journal of the Atmospheric Sciences*, *77*(12), 4233–4249. https://doi.org/10.1175/JAS-D-20-0111.1

Schumacher, R. S., & Rasmussen, K. L. (2020). The formation, character and changing nature of mesoscale convective systems. *Nature Reviews Earth & Environment*, *1*(6), 300–314. https://doi.org/10.1038/s43017-020-0057-7

Semie, A. G., & Bony, S. (2020). Relationship between precipitation extremes and convective organization inferred from satellite observations. *Geophysical Research Letters*, *47*(9), e2019GL086927. https://doi.org/10.1029/2019GL086927

Serra, Y. L., Rutledge, S. A., Chudler, K., & Zhang, C. (2023). Rainfall and convection in ERA5 and MERRA-2 over the northern equatorial western pacific during PISTON. *Journal of Climate*, *36*(3), 845–863. https://doi.org/10.1175/JCLI-D-22-0203.1

Simpson, J., Kummerow, C., Tao, W. K., & Adler, R. F. (1996). On the tropical rainfall measuring mission (TRMM). *Meteorology and Atmospheric Physics*, *60*(1–3), 19–36. https://doi.org/10.1007/BF01029783

Skofronick-Jackson, G., Petersen, W. A., Berg, W., Kidd, C., Stocker, E. F., Kirschbaum, D. B., et al. (2017). The global precipitation measurement (GPM) mission for science and society. *Bulletin America Meteorology Social*, *98*(8), 1679–1695. https://doi.org/10.1175/BAMS-D-15-00306.1

Stevens, B., Bony, S., & Webb, M. (2012). Clouds on-off klimate intercomparion experiment (COOKIE). https://doi.org/10.1109/TBCAS.2011.2166962

Su, H., Bretherton, C. S., & Chen, S. S. (2000). Self-aggregation and large-scale control of tropical deep convection: A modeling study. *Journal of the Atmospheric Sciences*, *57*(11), 1797–1816. https://doi.org/10.1175/1520-0469(2000)057<1797:SAALSC>2.0.CO;2

Tan, J., Jakob, C., Rossow, W., & Tselioudis, G. (2015). Increases in tropical rainfall driven by changes in frequency of organized deep convection. *Nature*, *519*(7544), 451–454. https://doi.org/10.1038/nature14339

The MathWorks Inc. (2023). *MATLAB version: 23.2.0 (R2023b)*. The MathWorks Inc. Retrieved from https://www.mathworks.com

Tobin, I., Bony, S., Holloway, C. E., Grandpeix, J.-Y., Sèze, G., Coppin, D., et al. (2013). Does convective aggregation need to be represented in cumulus parameterizations? *Journal of Advances in Modeling Earth Systems*, *5*(4), 692–703. https://doi.org/10.1002/jame.20047

Tobin, I., Bony, S., & Roca, R. (2012). Observational evidence for relationships between the degree of aggregation of deep convection, water vapor, surface fluxes, and radiation. *Journal of Climate*, *25*(20), 6885–6904. https://doi.org/10.1175/JCLI-D-11-00258.1

Tomassini, L. (2020). The interaction between moist convection and the atmospheric circulation in the tropics. *Bulletin America Meteorology Social*, *101*(8), E1378–E1396. https://doi.org/10.1175/BAMS-D-19-0180.1

Tompkins, A. M., & Semie, A. G. (2017). Organization of tropical convection in low vertical wind shears: Role of updraft entrainment. *Journal of Advances in Modeling Earth Systems*, *9*(2), 1046–1068. https://doi.org/10.1002/2016MS000802

Trapp, R. J. (2013). *Mesoscale-convective processes in the atmosphere* (p. 346). Cambridge University Press.

Tsai, W., & Mapes, B. E. (2022). Evidence of aggregation dependence of 5°-scale tropical convective evolution using a gross moist stability framework. *Journal of the Atmospheric Sciences*, *79*(5), 1385–1404. https://doi.org/10.1175/JAS-D-21-0253.1

Voigt, A., Albern, N., Ceppi, P., Grise, K., Li, Y., & Medeiros, B. (2021). Clouds, radiation, and atmospheric circulation in the present-day climate and under climate change. *WIREs Clim Change*, *12*(2), e694. https://doi.org/10.1002/wcc.694

Webb, M. J., Andrews, T., Bodas-Salcedo, A., Bony, S., Bretherton, C. S., Chadwick, R., et al. (2017). The cloud feedback model Intercomparison project (CFMIP) contribution to CMIP6. *Geoscientific Model Development*, *10*(1), 359–384. https://doi.org/10.5194/gmd-10-359-2017

White, B. A., Buchanan, A. M., Birch, C. E., Stier, P., & Pearson, K. J. (2018). Quantifying the effects of horizontal grid length and parameterized convection on the degree of convective organization using a metric of the potential for convective interaction. *Journal of the Atmospheric Sciences*, *75*(2), 425–450. https://doi.org/10.1175/JAS-D-16-0307.1

Wielicki, B. A., Barkstrom, B. R., Harrison, E. F., Lee, R. B., Smith, G. L., & Cooper, J. E. (1996). Clouds and the Earth's radiant energy system (CERES): An Earth observing system experiment. *Bulletin of the American Meteorological Society*, *77*(5), 853–868. https://doi.org/10.1175/1520-0477(1996)077<0853:CATERE>2.0.CO;2

Wielicki, B. A., & Welch, R. M. (1986). Cumulus cloud properties derived using Landsat satellite radar. *Journal of Climate and Applied Meteorology*, *25*(3), 261–276. https://doi.org/10.1175/1520-0450(1986)025<0261:ccpdul>2.0.co;2

Wing, A. A., Emanuel, K., Holloway, C. E., & Muller, C. (2017). Convective self-aggregation in numerical simulations: A review. *Surveys in Geophysics*, *38*(6), 1173–1197. https://doi.org/10.1007/s10712-017-9408-4

Wing, A. A., & Emanuel, K. A. (2014). Physical mechanisms controlling self-aggregation of convection in idealized numerical modeling simulations. *Journal of Advances in Modeling Earth Systems*, *6*(1), 59–74. https://doi.org/10.1002/2013MS000269

Wing, A. A., Stauffer, C. L., Becker, T., Reed, K. A., Ahn, M.-S., Arnold, N. P., et al. (2020). Clouds and convective self-aggregation in a multimodel ensemble of radiative-convective equilibrium simulations. *Journal of Advances in Modeling Earth Systems*, *12*(9), e2020MS002138. https://doi.org/10.1029/2020MS002138

Wu, S.-N., Soden, B. J., & Nolan, D. S. (2021). Examining the role of cloud radiative interactions in tropical cyclone development using satellite measurements and WRF simulations. *Geophysical Research Letters*, *48*(15), e2021GL093259. https://doi.org/10.1029/2021GL093259

Xu, K.-M., & Randall, D. A. (1995). Impact of interactive radiative transfer on the macroscopic behavior of cumulus ensembles. Part II: Mechanisms for cloud–radiation interactions. *Journal of the Atmospheric Sciences*, *52*, 800–817. https://doi.org/10.1175/1520-0469(1995)052,0800:IOIRTO.2.0.CO;2

Yang, D. (2018a). Boundary layer diabatic processes, the virtual effect, and convective self-aggregation. *Journal of Advances in Modeling Earth Systems*, *10*(9), 2163–2176. https://doi.org/10.1029/2017ms001261

Yang, D. (2018b). Boundary layer height and buoyancy determine the horizontal scale of convective self-aggregation. *Journal of the Atmospheric Sciences*, *75*(2), 469–478. https://doi.org/10.1175/JAS-D-17-0150.1

Yao, L., & Yang, D. (2023). Convective self-aggregation occurs without radiative feedbacks in warm climates. *Geophysical Research Letters*, *50*(16), e2023GL104624. https://doi.org/10.1029/2023GL104624

Yuan, J., Houze, R. A., & Heymsfield, A. J. (2011). Vertical structures of anvil clouds of tropical mesoscale convective systems observed by CloudSat. *Journal of the Atmospheric Sciences*, *68*(8), 1653–1674. https://doi.org/10.1175/2011JAS3687.1

Zhang, B., Soden, B. J., Vecchi, G. A., & Yang, W. (2021). Investigating the causes and impacts of convective aggregation in a high resolution atmospheric GCM. *Journal of Advances in Modeling Earth Systems*, *13*(11), e2021MS002675. https://doi.org/10.1029/2021MS002675

Zhu, T., Lee, J., Weger, R. C., & Welch, R. M. (1992). Clustering, randomness, and regularity in cloud fields: 2. Cumulus cloud fields. *Journal of Geophysical Research*, *97*(D18), 20537–20558. https://doi.org/10.1029/92JD02022